Diverse structural solutions to catalysis in a family of antibodies

B Gigant[1], T Tsumuraya[2], I Fujii[2]* and M Knossow[1]*

Background: Small organic molecules coupled to a carrier protein elicit an antibody response on immunisation. The diversity of this response has been found to be very narrow in several cases. Some antibodies also catalyse chemical reactions. Such catalytic antibodies are usually identified among those that bind tightly to an analogue of the transition state (TSA) of the relevant reaction; therefore, catalytic antibodies are also thought to have restricted diversity. To further characterise this diversity, we investigated the structure and biochemistry of the catalytic antibody 7C8, one of the most efficient of those which enhance the hydrolysis of chloramphenicol esters, and compared it to the other catalytic antibodies elicited in the same immunisation.

Results: The structure of a complex of the 7C8 antibody Fab fragment with the hapten TSA used to elicit it was determined at 2.2 Å resolution. Structural comparison with another catalytic antibody (6D9) raised against the same hapten revealed that the two antibodies use different binding modes. Furthermore, whereas 6D9 catalyses hydrolysis solely by transition-state stabilisation, data on 7C8 show that the two antibodies use mechanisms where the catalytic residue, substrate specificity and rate-limiting step differ.

Conclusions: Our results demonstrate that substantial diversity may be present among antibodies catalysing the same reaction. Therefore, some of these antibodies represent different starting points for mutagenesis aimed at boosting their activity. This increases the chance of obtaining more proficient catalysts and provides opportunities for tailoring catalysts with different specificities.

Addresses: [1]Laboratoire d'Enzymologie et Biochimie Structurales, CNRS UPR 9063, Bat. 34 CNRS, 1 Avenue de la Terrasse, 91198 Gif-sur-Yvette Cedex, France and [2]Biomolecular Engineering Research Institute, 6-2-3 Furuedai, Suita, Osaka 565, Japan.

*Corresponding authors.
E-mail: fujii@bioorg.beri.co.jp
knossow@lebs.cnrs-gif.fr

Key words: oxyanion, phosphonate, prodrug, transition state analogue, X-ray structure

Received: 24 June 1999
Revisions requested: 10 August 1999
Revisions received: 24 August 1999
Accepted: 26 August 1999

Published: 29 October 1999

Structure November 1999, 7:1385–1393

0969-2126/99/$ – see front matter

Introduction

The concept that a higher affinity of an enzyme for a transition state compared with substrate increases the rate of the corresponding chemical reaction dates back to Pauling [1]. It was then predicted by Jencks that antibodies raised against a chemically stable transition-state analogue (TSA) could catalyse this reaction [2]. Since the first experimental reports of catalytic antibodies [3,4], more than 80 different antibody-catalysed reactions have been catalogued, corresponding to all but one of the major enzyme classes [5]. Although some antibodies have been reported to have an efficiency similar to or better than that of the corresponding enzyme [6], in a number of cases it has been difficult to obtain such high efficiencies using the approach proposed by Jencks, and improvement of catalytic antibody efficiency is one of the major challenges in the field [7]. Ways have been sought to boost this efficiency either by site-specific mutagenesis [8–10] or by a more systematic approach based on libraries of mutated antibodies [11]. As immunisation with a TSA hapten usually gives rise to several catalysts, the question arises of which antibody to choose as a starting point for engineering. When the binding modes of these catalysts are all very similar, modifications of any of them would be sufficient to explore all the possibilities for improvement; if the binding modes are dissimilar, mutagenesis of different antibodies might give rise to different optimised efficiencies.

The genetic diversity of the antibody response to a number of model haptens has been studied by sequence analysis and, in general, the response to simple epitopes is found to be very restricted and is characterised as idiotypic [12]. In a few cases these studies have been completed by determination of the structures of one or two of the elicited antibodies [13–15]. In one case, when sequences of antibodies specific for 2-phenyloxazolone were analysed in the context of the structure of one of them, the conclusion was reached that the immune system sees the hapten by a very limited number of principal mechanisms [15]; in another case, however, two binding modes were identified [13,14]. As catalytic antibodies are usually identified among those that bind tightly to the TSA hapten and as they undergo further screening for catalytic activity, their diversity of binding mode is expected to be even more restricted than that of hapten-binding antibodies. Antibodies resulting from a single immunisation have been defined as belonging to 'a family of antibodies'. A high degree of sequence identity between catalytic antibodies of the same family has been reported in several cases [16–18], and when structures were determined, they were found to have many similar features [19,20]. In contrast to

these findings, we report here the structure of a catalytic antibody that binds its corresponding TSA hapten in a mode that is totally different from that used by other catalytic antibodies recovered from the same immunisation.

Antibody 7C8 was raised against the chloramphenicol phosphonate derivative (**1**; Figure 1) and catalyses the hydrolysis of the corresponding ester (**2**) with significant rate enhancement to generate chloramphenicol (**3**) and the acid product [21]. Five other catalysts were recovered from the same immunisation. These five antibodies share a high degree of sequence similarity [22]. Antibody 6D9, the best of these five catalysts, was characterised in detail [21] and its structure determined by X-ray crystallography [23]. The degree of similarity of the 7C8 variable domain amino acid sequences to those of the other five antibodies is close to 50%; despite these differences, 7C8 is as efficient as 6D9 (k_{cat} values are 0.115 min^{-1} and 0.145 min^{-1}, respectively). We have determined the structure of the 7C8 Fab fragment (the antigen-binding fragment) complexed with the phosphonate transition state analogue **1** and show that antibodies 7C8 and 6D9 bind their common TSA hapten through different modes; this accounts for their different specificities. We also show that the catalytic residues involved and the rate-limiting steps, and therefore the mechanisms, of these two antibodies differ.

Results and discussion

Overview of the structure

The crystal structure of the 7C8 Fab was determined at 2.2 Å resolution. There are two Fab molecules in the asymmetric unit of the 7C8 crystal; the elbow angles of the two Fabs are in the observed range for antibodies but

Figure 1

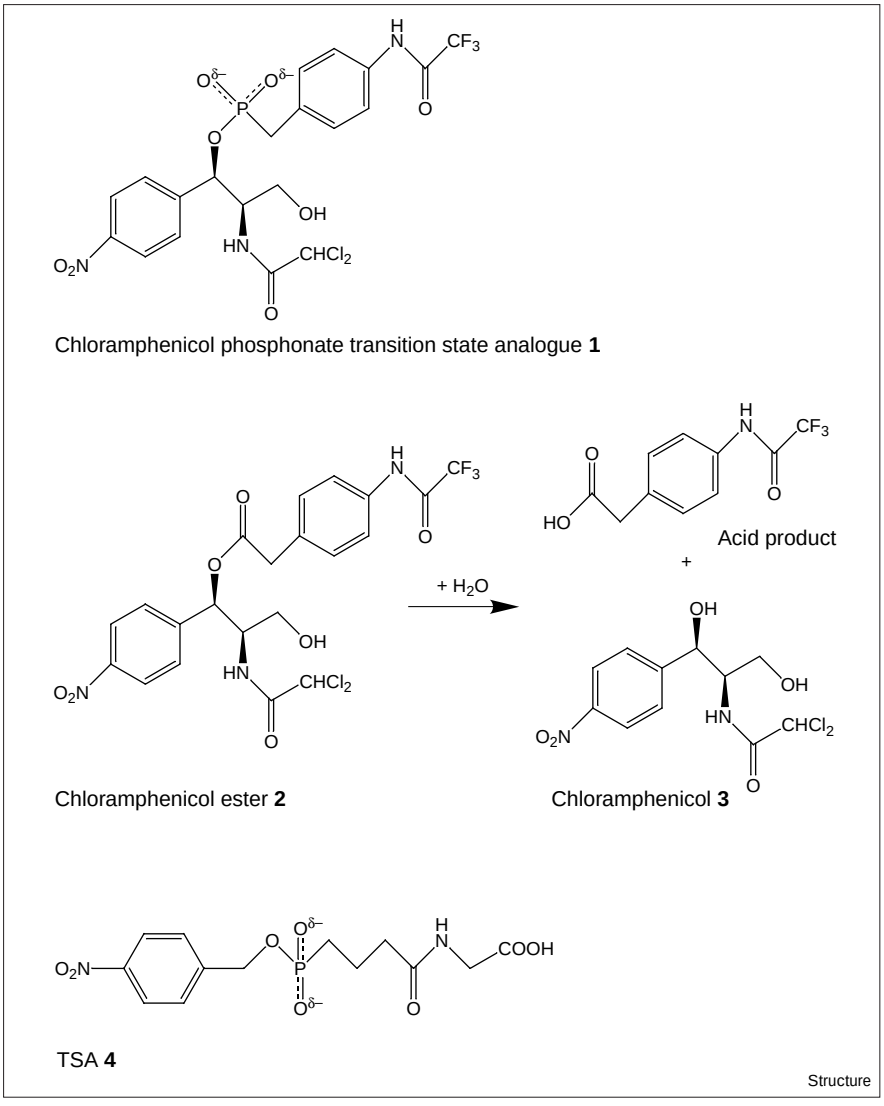

Chemical formulae of the compounds used in this study. Antibody 7C8 was raised against the chloramphenicol phosphonate **1** and catalyses the hydrolysis of the chloramphenicol ester **2** to generate the acid product and chloramphenicol **3**. TSA **4** was used to elicit the *p*-nitrobenzyl ester hydrolysing antibody D2.3 [49].

differ by 8°. Several other antibodies for which Fab structures have been determined by X-ray crystallography have been observed to adopt different elbow angles in each of the copies of their Fabs in the asymmetric unit [24]; the accumulated evidence therefore supports the idea that the elbow angle is influenced by the environment and in particular by crystal packing.

The overall shape of the antibody combining site (the antigen-binding site), where the hapten TSA **1** is located, is a shallow groove rather than the deep pocket commonly found in antibody structures whose antigen is a small hapten [25]. This results in only 60% of the surface area of the ligand being buried in the combining site and may account for the relatively high value of the dissociation constant K_d (0.3 μM) of the antibody for hapten **1** [21]. The trifluoroacetamide moiety of the hapten (Figure 2) and the attachment site for the carrier protein used for immunisation represent 75% of the surface remaining accessible after binding of **1** to the Fab. Probably because of its relatively limited contacts with the Fab, the trifluoroacetamide moiety of the hapten is in poorly defined electron density, and the temperature factor for this part of the ligand is significantly higher than the average B factor of the ligand (36 Å^2 versus 17 Å^2, averaged over the two molecules of the asymmetric unit). The contacts to this part of the hapten are made by two residues at the tip of the hypervariable loop H3; in H3 only two other residues, TyrH95 and PheH100a (where H denotes heavy chain; residue numbering is according to [26]), contact the hapten (Figure 2).

The structures of eight antiphosphonate hydrolytic antibodies belonging to four different families have been determined previous to those of the 7C8/6D9 family. It was noticed that the related hapten ligands of these antibodies, which all comprise an aryl phosphonate moiety, are bound in such a way that their aromatic part is deeply buried in a semiconserved hydrophobic pocket of the antibody combining site at the interface of the heavy- and light-chain variable domains [27]. Here, as in 6D9 [23], the hapten is

Figure 2

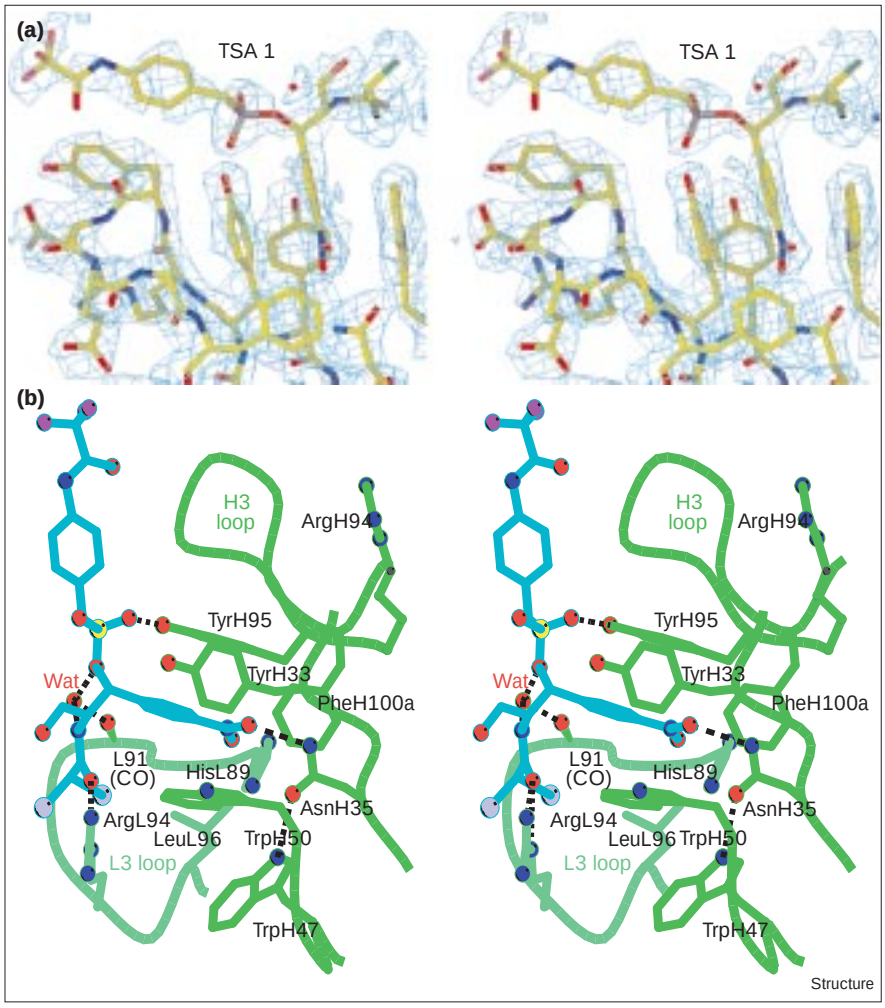

The antibody 7C8–TSA 1 interface. (a) Stereoview of a $2F_o–F_c$ electron-density map contoured at the 1σ level in the combining site of one of the Fab molecules in the asymmetric unit. The contribution of the atoms of the hapten was omitted in the calculation of the map. Atoms are colour coded: carbon, yellow; nitrogen, blue; oxygen, red; chlorine, green; fluorine, pink; phosphorus, magenta. (b) Schematic stereoview of the 7C8 active site (in green) in complex with TSA 1 (in blue). Atoms are colour coded: chlorine, grey; fluorine, purple; and phosphorus, yellow. A water molecule is shown as a red sphere and labelled (Wat). Hydrogen bonds are shown as broken lines. Only residues discussed in the text are represented. (Part (a) was rendered in the program O [43]; part (b) was rendered with the program MOLSCRIPT [50].)

Figure 3

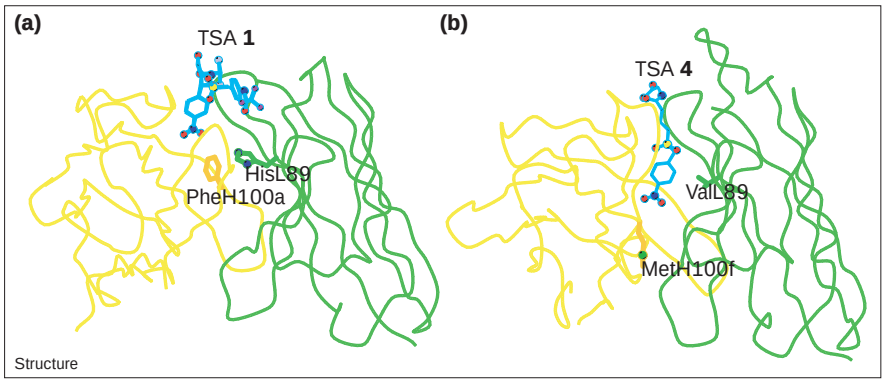

Comparison of the location of (a) the hapten 1 in the active site of 7C8 and (b) the hapten 4 in the combining site of antibody D2.3 [19]. The ligands are drawn in blue, heavy chains are in yellow and the light chains in green. In 7C8, the sidechains of residues L89 and H100a that prevent deeper burying of the nitro group of the hapten are represented; residues labelled in D2.3 are the equivalent residues identified from the superposition of 7C8 with D2.3. (The figure was rendered with the program MOLSCRIPT [50].)

bound on the surface of the combining site and its nitro group, although completely buried in the antibody, is displaced by 6 Å towards the outside of the site as compared with the equivalent group in the complex of antibody D2.3 with its hapten (Figure 3). Accordingly, in D2.3, which is representative of the hapten-binding mode of the four families of catalytic antibodies studied previously [27], the hapten buries 90% of its surface in contrast to 60% in 7C8.

To gain further insight into the reason for the different binding modes observed in 7C8 and other esterase-like antibodies, antibody D2.3 was used as their prototype. The *p*-nitrobenzyl and phosphonate groups of **1** and of the D2.3 hapten TSA **4** in its complex with D2.3 were superimposed; when this is done, one finds that the substituents to the benzylic carbon of **1** are too bulky to be accommodated in the D2.3 combining site. Such a superposition would, in particular, cause steric hindrance between the light-chain framework and the dichloroacetamide group of **1** (data not shown); therefore the structure adopted by 7C8 differs from that of D2.3. The deeply buried pocket of the combining site occupied by the NO_2 group in all the complexes of esterase-like catalytic antibodies studied previously is closed by two residues in 7C8. These residues are HisL89, provided by complementarity-determining region (CDR) L3, and PheH100a, which belongs to the bulge found in CDR H3 of 7C8 as well as in all H3 loops with an arginine or a lysine at position H94 [28]. By comparison, in D2.3, residue L89 (where L denotes light chain) is a valine, much smaller than histidine, and the bulge of the H3 loop is oriented such that the sidechain of residue 100f, which corresponds to H100a in 7C8 when 7C8 and D2.3 are superimposed, faces towards the outside of the antibody (Figure 3), whereas in 7C8 the H100a sidechain points towards the combining site (Figure 2).

The hapten–antibody interface: structural basis for substrate specificity

The substrate specificity of 7C8 has been established [21]; it is accounted for by the structure of the 7C8–TSA **1** complex. This is best analysed by considering in turn the four substituents that surround the phosphonate of **1** and mimicking the reaction centre of the ester to be hydrolysed (Figure 2). Substitutions at positions of the substrate equivalent to atoms in the hapten that have little contact with the Fab allow catalysis to be maintained. First, the hydroxyl group involved in the attachment of the hapten to the carrier protein does not interact with the antibody combining site. A modification of this hydroxyl has little effect on the rate enhancement and on the Michaelis constant K_M. Second, in the same way, the conversion of the trifluoroacetyl group to an acetyl group is also without consequence, in agreement with the limited contacts of this part of the hapten with the antibody. On the contrary, the *p*-nitrobenzyl group of **1** points towards the inside of the combining site and makes tight interactions with the Fab: the aromatic ring is stacked between the sidechains of TyrH95 and TrpH50 and the nitro group establishes a hydrogen bond with the AsnH35 sidechain. Consistently, the introduction of a bulky *p*-dichloroacetamide function instead of the *p*-nitro group results in an ester which is not a substrate of antibody 7C8.

Finally, the dichloroacetamide moiety of **1** is located on the surface of the antibody and its interactions with 7C8 influence the catalytic properties in a more subtle way than those of the trifluoroacetyl and *p*-nitrobenzyl groups. The dichloroacetamide group establishes van der Waals contacts and two hydrogen bonds with the L3 hypervariable loop of the antibody; additional interactions are mediated by a water molecule (Figure 2). The substitution of the dichloroacetamide by an acetylamide group results in a tenfold reduction of hydrolytic activity but in an identical K_M value. The substitution involves a group that is separated from the reaction centre by six covalent bonds. Interactions of a biocatalyst with substrate atoms distant from the reaction centre that contribute to rate acceleration and do not affect substrate binding have been observed in enzymes and in serine proteases in particular [29] and have also been documented in the case of

Figure 4

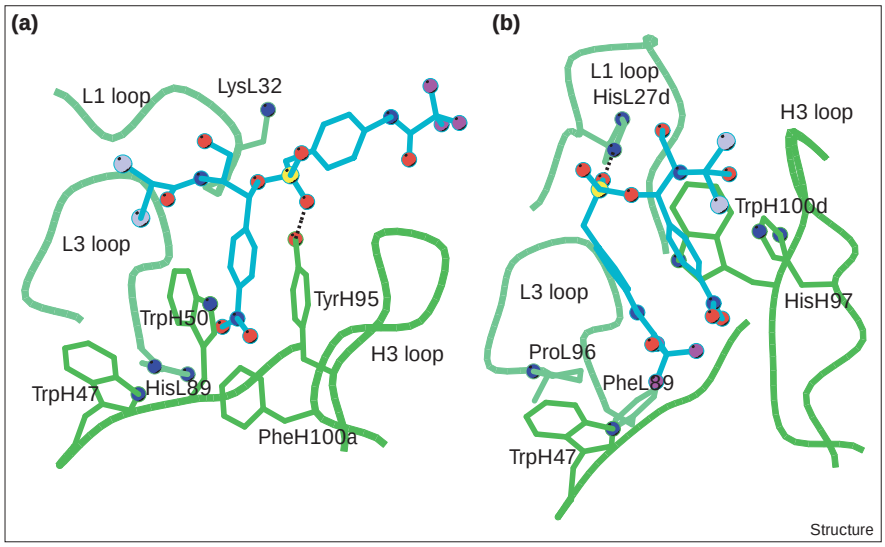

Comparison of the conformation of TSA **1** in the active site of (a) 7C8 and (b) 6D9 (same colour code as in Figure 2b). The combining sites are shown in the same orientation. In each case, the hydrogen bond established with the phosphonyl oxygen by the residue identified as catalytic is represented by a broken line. (The figure was rendered with the program MOLSCRIPT [50].)

a catalytic antibody [30]. 7C8 provides another example of an interaction at a distance from the reaction centre that affects catalysis, a feature reminiscent of enzymes.

Although they were elicited in the same immunisation, antibodies 6D9 and 7C8 accommodate their common hapten **1** in different ways (Figure 4). It is noteworthy that the TSA **1** has two distinct conformations in these antibodies. Whereas it is extended in the 7C8–TSA **1** structure, it is folded in the 6D9–TSA **1** complex, with its two aromatic rings stacked. As a consequence of the different binding modes of 7C8 and 6D9 their substrate specificities differ. Whereas 7C8 accepts significant changes to the acetyl substituent of its substrate, this is not the case for 6D9. This is accounted for by the structures: in the 7C8–TSA **1** structure the trifluoroacetyl group is exposed to the solvent whereas it is deeply buried in the 6D9–TSA **1** complex.

The most efficient antibodies of the 7C8/6D9 family use different catalytic mechanisms

Ester hydrolysis at alkaline pH involves the formation of an oxyanion intermediate which subsequently decomposes to the acid and alcohol products. Phosphonate TSAs have been designed to mimic this intermediate; the antibodies they elicit stabilise the phosphonate TSA and presumably the oxyanionic transition state better than the ester bond of the substrate and the target reaction is therefore catalysed. This principle has been ratified by all the structures of esterase-like antibodies determined so far [27,31]. Antibodies 6D9 and 7C8 bind the phosphonate of TSA **1** by establishing one hydrogen bond with it, whereas the second phosphonyl oxygen remains accessible to solvent after complex formation both in 6D9 and 7C8. As the structures differ, the residues providing the hydrogen bond donor group are different. In 6D9, a histidine of CDR L1 provides the hydrogen-bond to the phosphonate of **1** and has been shown by site-specific mutagenesis [32] to be the main residue responsible for catalysis. In 7C8, TyrH95 is the hydrogen-bond donor (Figure 2). The pH profile of the 7C8-catalysed reaction rate (Figure 5) shows an acid limb below pH 9 and is consistent with the involvement of TyrH95 in the mechanism. Apart from the catalytic residue, another feature differentiates catalysis by 7C8 and 6D9: addition of hydroxylamine, a better

Figure 5

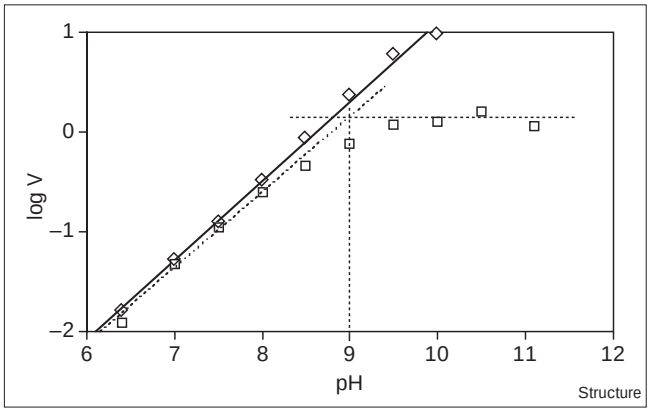

The pH dependence of the rate of catalysis (V) of substrate **2** hydrolysis by the antibodies 7C8 (large squares) and 6D9 (small diamonds) (for details, see the Materials and methods section). The logarithm of the 6D9 rate is a linear function of pH in the range explored, whereas that of the 7C8 rate shows an acid limb at pH 9. This observation is consistent with the participation of a tyrosine residue in the catalytic mechanism of 7C8.

Figure 6

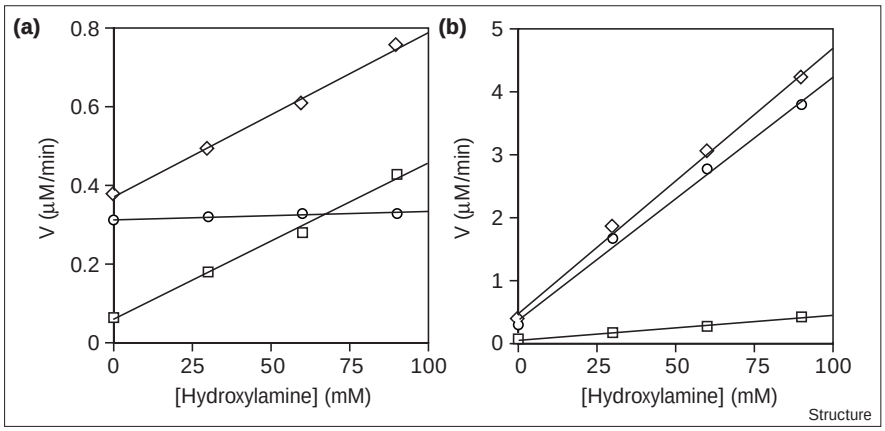

The effect of hydroxylamine on the catalytic activity of (a) 7C8 and (b) 6D9. For experimental details, see the Materials and methods section. Small diamonds, overall rate; large squares, background rate without antibody; small circles, catalysed reaction rate. The velocity of the 6D9-catalysed reaction is enhanced by hydroxylamine, whereas that of the 7C8-catalysed reaction is unaffected by this compound.

nucleophile than the hydroxide ion, enhances the rate of hydrolysis of ester **2** by 6D9 but leaves that of 7C8 unaffected (Figure 6). This shows that, in contrast to 6D9, nucleophilic attack by an hydroxide ion is not the rate-limiting step in catalysis by 7C8.

Whereas the kinetic data in conjunction with the 7C8–TSA **1** structure identify TyrH95 as one of the residues involved in catalysis, the exact role of this residue is more ambiguous. The pH profile is consistent both with TyrH95 being part of the oxyanion hole and with it having the role of a nucleophile. In the first case, TyrH95 would participate in catalysis by stabilising the transient oxyanion during ester hydrolysis, as planned by the TSA hapten. In this case, the nucleophile is an hydroxide ion; the rate is a function both of hydroxide ion concentration and of the proportion of TyrH95 that is protonated. Above its pK_a, TyrH95 becomes deprotonated, and this accounts for the plateau of the pH profile at high pH. If oxyanion stabilisation was the actual mechanism used by 7C8, the simplest interpretation of the pH profile suggests that OH^- attack would be the rate-determining step, which is inconsistent with the insensitivity of the rate to the addition of hydroxylamine. Therefore one needs to consider an alternative mechanism consistent with the pH rate profile, namely that in which TyrH95 is a nucleophile. In this case, the pH profile can be interpreted as follows: the tyrosine becomes a better nucleophile as it gets deprotonated and the rate would reach a plateau when deprotonation is complete. With this mechanism, the insensitivity of the rate to addition of hydroxylamine means that the rate-determining step is likely to be the nucleophilic attack by deprotonated tyrosine. For nucleophilic attack by TyrH95 to be a possible mechanism, the observed catalytic rate must be consistent with known values of the rates of all steps of this mechanism, and in particular with that of TyrH95 deacylation. The rate of the 7C8-catalysed reaction is approximately 100 times faster than the rate of uncatalysed hydrolysis of model tyrosine esters [33,34] so that, in order for nucleophilic attack by TyrH95 to be the major cause of catalysis by 7C8, deacylation of this residue needs to be assisted. A movement of the LysL32 sidechain (Figure 4) would bring it into a position to assist water activation. Unless this movement, or another structural rearrangement of the combining site, occurs during the reaction that positions a residue correctly to assist deacylation, a more complex mechanism would need to be advocated.

Biological implications

The diversity that allows protection against an enormous variety of unrelated pathogens is one of the fundamental properties of the antibody repertoire. Despite this, the diversity of the antibodies elicited by haptens is restricted, as is the diversity of the families of catalytic antibodies studied to date. In contrast to these findings, we identify here two different substrate-binding modes in a family of antibodies that hydrolyse chloramphenicol esters.

Chloramphenicol inhibits bacterial growth by binding to the 50S subunit of the ribosome, an effect which is prevented when this antibiotic is acetylated. Chloramphenicol and its monoester derivatives therefore constitute a good model system for the catalytic antibody approach to prodrug activation. With this goal in mind, a family of antibodies has been elicited by immunisation with a phosphonate transition-state analogue of chloramphenicol monoester hydrolysis. These antibodies catalyse this reaction with significant rate enhancement and multiple turnovers and the most efficient of them inhibits bacterial growth when the medium is supplemented with this chloramphenicol monoester.

Although the hapten used to elicit this family of antibodies contains proximal aromatic and phosphonate groups, as do all the haptens used so far to elicit esterase-like

antibodies that have been studied structurally, the binding modes used by these chloramphenicol-hydrolysing antibodies differ from the common binding mode identified in all other esterase-like antibodies. Moreover, the binding modes of the two most efficient antibodies differ from each other and, as a consequence, their specificities, rate-limiting steps and catalytic residues are different as well. This demonstrates that, at least in this case, several catalytic solutions are elicited through the immune response to a transition-state analogue hapten. These antibodies represent distinct starting points for the designed improvement of the efficiency of these catalysts and each one provides additional opportunities for reaching a higher optimised efficiency.

Finally, because of the way they were selected, the catalytic antibodies studied here represent a subset of those that efficiently bind a transition-state analogue hapten. Therefore, the diversity we identified applies not only to catalytic antibodies but more generally to the binding modes provided by the immune system in response to a single hapten molecule.

Materials and methods

Purification, crystallisation and data collection

The 7C8 antibody was purified from the ascitic fluid as described [35]. The Fab was generated by papain digestion of the antibody in standard conditions (30 mM Tris pH 7.4, 138 mM NaCl, 1.25 mM EDTA, 1.5 mM 2-mercaptoethanol) using a 3% papain to antibody ratio (w/w) and a 8.5 h digestion time. The Fab was purified by DEAE anion exchange chromatography followed by gel filtration.

For crystallisation, the Fab in 150 mM NaCl was concentrated to 5 mg/ml and complexed with TSA in a 1.1 M excess. Initial conditions yielding small twinned crystals were identified by sparse matrix screening [36]. The precipitant identified by this procedure comprised: 30% (w/v) polyethylene glycol (PEG) 8000, 0.2 M ammonium sulphate pH 4. Single crystals were obtained in 22% to 26% (w/v) PEG 1000, 0.2 M ammonium sulphate pH 4, following streak-seeding and macro-seeding.

A data set (data set 1) collected on a Rigaku R200 rotating-anode generator equipped with an Raxis II image-plate system was used for molecular replacement. Higher resolution data (up to 2.2 Å) were collected at the W32 station of the LURE synchrotron (Orsay, France) on a Mar-Research image-plate (data set 2). Both data sets were indexed and integrated with DENZO and scaled and merged with SCALEPACK [37]. Data collection statistics are summarised in Table 1.

Structure determination and refinement

The 7C8 Fab crystallises in the $P2_1$ space group; the unit-cell dimensions suggest that there are two Fab molecules in the asymmetric unit. The 7C8 Fab structure was solved by molecular replacement using data from data set 1 between 15 Å and 4 Å, with the program AMoRe [38]. The search models were the constant and the variable domains of the anti-lysozyme antibody D44.1 [39] taken separately (PDB code 1MLB [40]). This antibody was chosen from those for which Fabs are structurally known because it has the highest sequence similarity with 7C8, as detected by the program BLAST [41]. After molecular replacement, the R factor was 41%. We then alternated refinement using the conjugate gradient facility of X-PLOR [42] and reconstruction with the program O [43]. Progress of the refinement was judged by the decrease of the free R factor [44], calculated with 5% of the observations that were not included in the refinement. During refinement, we applied noncrystallographic symmetry restraints separately between the two Fvs (variable domains dimers) of the asymmetric unit on the one hand and between the two constant domains of the asymmetric unit on the other. This accounts for the fact that the elbow angles of the two Fabs differ (134° and 142°, respectively). The restraints were strict during the first rounds of refinement (at this stage the rmsd between the equivalent domains of the two Fabs of the asymmetric unit was less than 0.03 Å), and were subsequently relaxed as long as this improved the free R factor [45]. The hypervariable loops were reconstructed in $2F_o–F_c$ and $F_o–F_c$ omit maps. When all the residues had been incorporated, temperature factor refinement and coordinate refinement were performed alternately. The ligand constructed manually in the density in the antibody combining site was then incorporated into the refinement process. Its position was initially defined by the three highest peaks in a $F_o–F_c$ map, which were attributed to its phosphorus and two chlorine atoms. Water molecules were identified at positions above four standard deviations in this map, and one peak per Fab was attributed to a sulphate ion, consistent with the shape of the electron density and with the ions present in the crystallisation buffer. Refinement statistics are presented in Table 2. At the end of the refinement, more than 86% of the residues of 7C8 Fab have ψ and ϕ dihedral angles in the most favourable regions of the Ramachandran plot, as evaluated with the program PROCHECK [46]. There are three outliers: two of them are in a loop of the constant region for which there is no density, the other one is the residue L51 of the L2 CDR, which adopts in 7C8 the ubiquitous conformation of this residue in antibodies [47].

Table 1

Diffraction data statistics.

	Data set 1	Data set 2
Wavelength (Å)	1.54	0.97
Resolution limit (Å)	2.8	2.2
Observations	35,325	98,277
Unique reflections	18,796	40,238
Completeness (%)*	91.4 (73.3)	97.9 (95.7)
R_{sym} (%)*†	8.6 (27.6)	6.6 (25.3)
$I/\sigma(I)$*	9.3 (2.7)	15.2 (5.4)

Unit-cell dimensions for both data sets were a = 54.6 Å, b = 65.6 Å, c = 117.8 Å, β = 95.6° (α = γ = 90°). *Values in parentheses are for the highest resolution shell. †$R_{sym} = \Sigma\Sigma_j|I_j–\langle I\rangle|/\Sigma|\langle I\rangle|$, where I_j is the intensity measurement for reflection j and $\langle I\rangle$ is the mean intensity for multiply recorded reflections.

Superposition of atomic models was done with program O [43]. Accessible surface areas were calculated using the algorithm of Shrake and Rupley [48].

Dependence of the rate of catalysis on pH

The variation of the initial rate of hydrolysis of substrate **2** catalysed by antibodies 7C8 and 6D9 as a function of pH was determined between pH 6.4 and 11.1 in ATE buffer (100 mM ACES, 52 mM Tris, 52 mM ethanolamine). Reactions were initiated by adding 10 µl of a 2 mM solution of substrate **2** in DMSO to 90 µl of 1.1 µM antibody solution in ATE buffer at 25°C (final concentrations of substrate and antibody are 200 µM and 1.0 µM, respectively). Hydrolysis rates were measured by high pressure liquid chromatography (HPLC) analysis of the products in 10 µL aliquots of the reaction mixture as described [21] and were corrected for the uncatalysed rate of hydrolysis in the absence of antibody.

Hydroxylamine partitioning studies

The following stock solutions were prepared: 5 mM chloramphenicol ester **2** in DMSO; 1.67 µM antibody (7C8 or 6D9) in 50 mM Tris-HCl pH 8.0; 300 mM hydroxylamine in 50 mM Tris-HCl pH 8.0. Initial rate measurements were carried out at 25 °C in reaction volumes made up with 0–30 µl of hydroxylamine stock solution, 60 µl antibody stock

Table 2

Refinement statistics.

Resolution (Å)	14.3–2.2
R (%)*†	21.1 (30.0)
R_{free} (%)*	27.5 (36.8)
Water molecules	195
B factor (all atoms) (Å^2)	26
Rmsd from ideality	
bond lengths (Å)‡	0.011
bond angles (°)‡	1.75
Rmsd from noncrystallographic symmetry (Å)§	0.11
Rms coordinate error (Å)#	0.33

*Values in parentheses are for the highest resolution shell. †$R = \Sigma||F_{obs}|-|F_{calc}||/\Sigma|F_{obs}|$. ‡Evaluated using the program X-PLOR [42]. §Root mean square deviation (rmsd) between the two Fab fragments of the asymmetric unit related by noncrystallographic symmetry (evaluated with X-PLOR [42]). #Evaluated with Sigmaa [51].

solution and completed to 90 µl with reaction buffer (50 mM Tris-HCl pH 8.0). Reactions were initiated by adding 10 µl substrate stock solution to the mixture. Formation of chloramphenicol was measured by HPLC as described above.

Accession numbers

The coordinates have been deposited in the Protein Data Bank with accession code 1CT8.

Acknowledgements

We thank L Tchertanova (ICSN, CNRS, Gif-sur-Yvette) for surveying the Cambridge Data Base and J Perez for helping us to use facilities at LURE, Orsay, France. This work was supported by EU-TMR grant ERBFMXCT 98-0193 (MK).

References

1. Pauling, L. (1948). Nature of forces between large molecules of biological interest. *Nature* **161**, 707-709.
2. Jencks, W.P. (1969). *Catalysis in Chemistry and Enzymology*. McGraw-Hill, New York.
3. Tramontano, A., Janda, K.D. & Lerner, R.A. (1986). Catalytic antibodies. *Science* **234**, 1566-1570.
4. Pollack, S.J., Jacobs, J.W. & Schultz, P.G. (1986). Selective chemical catalysis by an antibody. *Science* **234**, 1570-1572.
5 Thomas, N.R. (1996). Catalytic antibodies – Reaching adolescence? – Reviewing the literature published up to the end of February 1996. *Nat. Prod. Rep.* **13**, 479-511.
6. Barbas, C.F. *et al.*, & Lerner, R.A. (1997). Immune versus natural selection: antibody aldolases with enzymic rates but broader scope. *Science* **278**, 2085-2092.
7. Driggers, E.M. & Schultz, P.G. (1996). Catalytic antibodies. *Adv. Protein Chem.* **49**, 261-287.
8. Stewart, J.D., Roberts, V.A., Thomas, N.R., Getzoff, E.D. & Benkovic, S.J. (1994). Site-directed mutagenesis of a catalytic antibody: an arginine and a histidine residue play key roles. *Biochemistry* **33**, 1994-2003.
9. Baldwin, E. & Schultz, P.G. (1989). Generation of a catalytic antibody by site-directed mutagenesis. *Science* **245**, 1104-1107.
10. Fletcher, M.C., Kuderova, A., Cygler, M. & Lee, J.S. (1998). Creation of a ribonuclease abzyme through site-directed mutagenesis. *Nat. Biotechnol.* **16**, 1065-1067.
11. Baca, M., Scanlan, T.S., Stephenson, R.C. & Wells, J.A. (1997). Phage display of a catalytic antibody to optimize affinity for transition-state analog binding. *Proc. Natl Acad. Sci. USA* **94**, 10063-10068.
12. Milstein, C. & Neuberger, M.S. (1996). Maturation of the immune response. *Adv. Protein Chem.* **49**, 451-485.
13. Jeffrey, P.D. *et al.*, & Sheriff, S. (1993). 26-10 Fab-digoxin complex: affinity and specificity due to surface complementarity. *Proc. Natl Acad. Sci. USA* **90**, 10310-10314.
14. Jeffrey, P.D., Schildbach, J.F., Chang, C.-Y.Y., Kussie, P., Margolies, M.N. & Sheriff, S. (1995). Structure and specificity of the anti-digoxin antibody 40-50. *J. Mol. Biol.* **248**, 344-360.
15. Alzari, P.M. *et al.*, & Milstein, C. (1990). Three-dimensional structure determination of an anti-2-phenyloxazolone antibody: the role of somatic mutation and heavy/light chain pairing in the maturation of an immune response. *EMBO J.* **9**, 3807-3814.
16. Ulrich, H.D. & Schultz, P.G. (1998). Analysis of hapten binding and catalytic determinants in a family of catalytic antibodies. *J. Mol. Biol.* **275**, 95-111.
17. Guo, J., Huang, W., Zhou, W.G., Fletterick, R.J. & Scanlan, T.S. (1995). Mechanistically different catalytic antibodies obtained from immunization with a single transition-state analog. *Proc. Natl Acad. Sci. USA* **92**, 1694-1698.
18. Angeles, T.S. *et al.*, & Martin, M.T. (1993). Isoabzymes: structurally and mechanistically similar catalytic antibodies from the same immunization. *Biochemistry* **32**, 12128-12135.
19. Charbonnier, J.-B. *et al.*, & Knossow, M. (1997). Structural convergence seen in the active sites of a family of catalytic antibodies. *Science* **275**, 1140-1142.
20. Buchbinder, J.L., Stephenson, R.C., Scanlan, T.S. & Fletterick, R.J. (1998). A comparison of the crystallographic structures of two catalytic antibodies with esterase activity. *J. Mol. Biol.* **282**, 1033-1041.
21. Fujii, I., Tanaka, F., Miyashita, H., Tanimura, R. & Kinoshita, K. (1995). Correlation between antigen-combining-site structures and functions within a panel of catalytic antibodies generated against a single transition state analog. *J. Am. Chem. Soc.* **117**, 6199-6209.
22. Miyashita, H., Hara, T., Tanimura, R., Tanaka, F., Kikuchi, M. & Fujii, I. (1994). A common ancestry for multiple catalytic antibodies generated against a single transition-state analog. *Proc. Natl Acad. Sci. USA* **91**, 6045-6049.
23. Kristensen, O., Vassylyev, D.G., Tanaka, F., Morikawa, K. & Fujii, I. (1998). A structural basis for transition-state stabilization in antibody-catalyzed hydrolysis: crystal structures of an abzyme at 1.8 Å resolution. *J. Mol. Biol.* **281**, 501-511.
24. Wilson, I.A. & Stanfield, R.L. (1994). Antibody–antigen interactions: new structures and new conformational changes. *Curr. Opin. Struct. Biol.* **4**, 857-867.
25. Brändén, C. & Tooze, J. (1991). *Introduction to Protein Structure*. Garland, New York.
26. Kabat, E.A., Wu, T.T., Perry, H.M., Gottesman, K.S. & Foeller, C. (1991). *Sequences of Proteins of Immunological Interest.* National Institute of Health, Bethesda, MD.
27. Charbonnier, J.-B., Gigant, B., Golinelli-Pimpaneau, B. & Knossow, M. (1997). Similarities of hydrolytic antibodies revealed by their X-ray structures: a review. *Biochimie* **79**, 653-660.
28. Morea, V., Tramontano, A., Rustici, M., Chothia, C. & Lesk, A.M. (1998). Conformations of the third hypervariable region in the V_h domain of immunoglobulins. *J. Mol. Biol.* **275**, 269-294.
29. Fersht, A.R. (1985). *Enzyme Structure and Mechanism.* W.H. Freeman, New York.
30. Gigant, B., Charbonnier, J.B., Eshhar, Z., Green, B.S. & Knossow, M. (1998). Crossreactivity, efficiency and catalytic specificity of an esterase-like antibody. *J. Mol. Biol.* **284**, 741-750.
31. MacBeath, G. & Hilvert, D. (1996). Hydrolytic antibodies: variations on a theme. *Chem. Biol.* **3**, 433-445.
32. Miyashita, H. *et al.*, & Fujii, I. (1997). Site-directed mutagenesis of active site contact residues in a hydrolytic abzyme: evidence for an essential histidine involved in transition-state stabilization. *J. Mol. Biol.* **267**, 1247-1257.
33. Martin, M.T., Napper, A.D., Schultz, P.G. & Rees, A.R. (1991). Mechanistic studies of a tyrosine-dependent catalytic antibody. *Biochemistry* **30**, 9757-9761.
34. Guo, J., Huang, W. & Scanlan, T.S. (1994). Kinetic and mechanistic characterization of an efficient hydrolytic antibody: evidence for the formation of an acyl intermediate. *J. Am. Chem. Soc.* **116**, 6062-6069.
35. Miyashita, H., Karaki, Y., Kikuchi, M. & Fujii, I. (1993). Prodrug activation via catalytic antibodies. *Proc. Natl Acad. Sci. USA* **90**, 5337-5340.
36. Jancarik, J. & Kim, S. (1991). Sparse matrix sampling: a screening method for crystallization of proteins. *J. Appl. Cryst.* **24**, 409-411.
37. Otwinowsky, Z. & Minor, W. (1997). *Processing of X-Ray Diffraction Data Collected in Oscillation Mode. Methods Enzymol.* **276**, 307-325.
38. Navaza, J. (1994). AMoRe: an automated package for molecular replacement. *Acta. Crystallogr. A* **50**, 157-163.
39. Braden, B.C., *et al.*, & Poljak, R. (1994). Three-dimensional structures of the free and the antigen-complexed Fab from monoclonal anti-lysozyme antibody D44.1. *J. Mol. Biol.* **243**, 767-781.

40. Bernstein, F.C. & Tasumi, M. (1977). A computer based archival file for macromolecular structures. *J. Mol. Biol.* 112, 535-542.
41. Altschul, S.F., Gish, W., Miller, W., Myers, E.W. & Lipman, D.J. (1990). Basic local alignment search tool. *J. Mol. Biol.* 215, 403-410.
42. Brünger, A.T. (1992). *X-PLOR (Version 3.1) Manual.* Yale University, New Haven, CT.
43. Jones, T.A., Zhou, J.-Y., Cowan, S.W. & Kjeldgaard, M. (1991). Improved methods for building protein models in electron density maps and the location of errors in these models. *Acta Crystallogr. A* 47, 110-119.
44. Brünger, A.T. (1992). Free R value: a novel statistical quantity for assessing the accuracy of crystal structures. *Nature* 355, 472-475.
45. Kleywegt, G.J. & Brünger, A.T. (1996). Checking your imagination: applications of the free R value. *Structure* 4, 897-904.
46. Laskowski, R.A., McArthur, M.W., Moss, D.S. & Thornton, J.M. (1993). PROCHECK: a program to check the stereochemical quality of protein structures. *J. Appl. Crystallogr.* 26, 283-291.
47. Al-Lazikani, B., Lesk, A.M. & Chothia, C. (1997). Standard conformations for the canonical structures of immunoglobulins. *J. Mol. Biol.* 273, 927-948.
48. Shrake, A. & Rupley, J.A. (1973). Environment and exposure to solvent of proteins atoms. Lysozyme and insulin. *J. Mol. Biol.* 79, 351-371.
49. Tawfik, D.S., Green, B.S., Chap, R., Sela, M. & Eshhar, Z. (1993). CatELISA: A facile general route to catalytic antibodies. *Proc. Natl Acad. Sci. USA* 90, 373-377.
50. Kraulis, P. (1991). MOLSCRIPT: a program to produce both detailed and schematic plots of proteins structures. *J. Appl. Crystallogr.* 24, 924-950.
51. CCP4 (1994). The CCP4 suite: programs for protein crystallography. *Acta Crystallogr. D* 50, 760-763.

Because *Structure with Folding & Design* operates a 'Continuous Publication System' for Research Papers, this paper has been published on the internet before being printed (accessed from http://biomednet.com/cbiology/str). For further information, see the explanation on the contents page.